Electronic Supplementary Material (ESI) for Soft Matter.

SUPPLEMENTARY INFORMATION

Title

Magnetically Induced Stiffening in Soft Robotics

Authors

Leah T. Gaeta,[a] Kevin J. McDonald,[a] Lorenzo Kinnicutt,[a] Megan Le ,[a] Sidney Wilkinson-Flicker,[a] Yixiao Jiang,[a] Taylan Atakuru,[b] Evren Samur,[b] and Tommaso Ranzani*[a,c,d]

Affiliations

[a] Department of Mechanical Engineering, Boston University, Boston, MA 02215, USA.
[b] Department of Mechanical Engineering, Boğaziçi University, Istanbul, Turkey.
[c] Division of Materials Science and Engineering, Boston University, Boston, MA 02215, USA.
[d] Department of Biomedical Engineering, Boston University, Boston, MA 02215, USA.

This file includes:

S1 Experiment Samples & Testing Set-Up

A picture of the MRJ beams tested in the manuscript is reported in Fig. S1 A. Fig. S1 B shows the cross-sectional view of the inside of an MRJ beam with laminar scaffolding.

In Fig. S2 we show the MRJ beam during a three point bending test. The magnets' location has been drawn and overlapped with the picture because the elastomer housing is not transparent. In Fig. S3 we report pictures taken during testing MRJ beams without magnetic field (Fig. S3 A), with a single row of magnets (Fig. S3 B), and with the double row of magnets (Fig. S3 C). A drawing of the magnets' location during testing is overlapped with the picture. As shown in Figs. S2 and S3, during the bending stiffness tests the anvil applies a force in the location between the magnets.

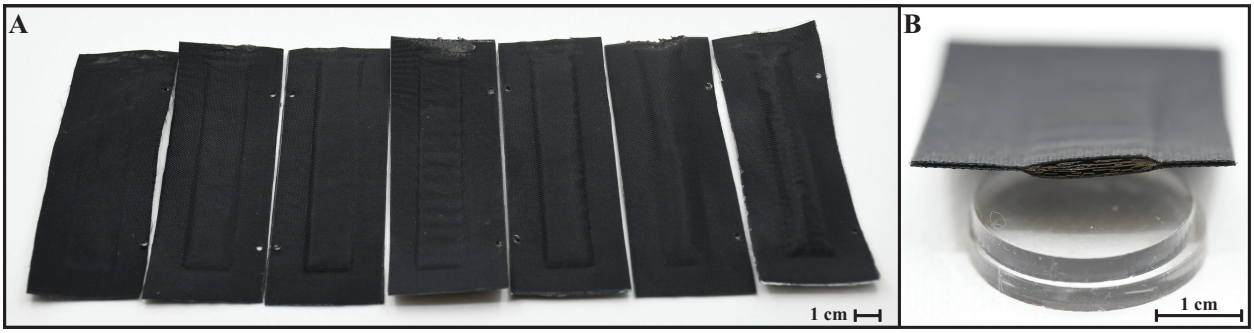

Figure S1: (A) MRJ beams used during experiments. Scaffolding architectures, left to right: none, "blanks" 10 layers, "blanks" 20 layers, "dots" 10 layers, "dots" 20 layers, fibers, and granules. (B) Cross-sectional view of the "dots" 10 layers MRJ beam with MRF seen surrounding and between the layers.

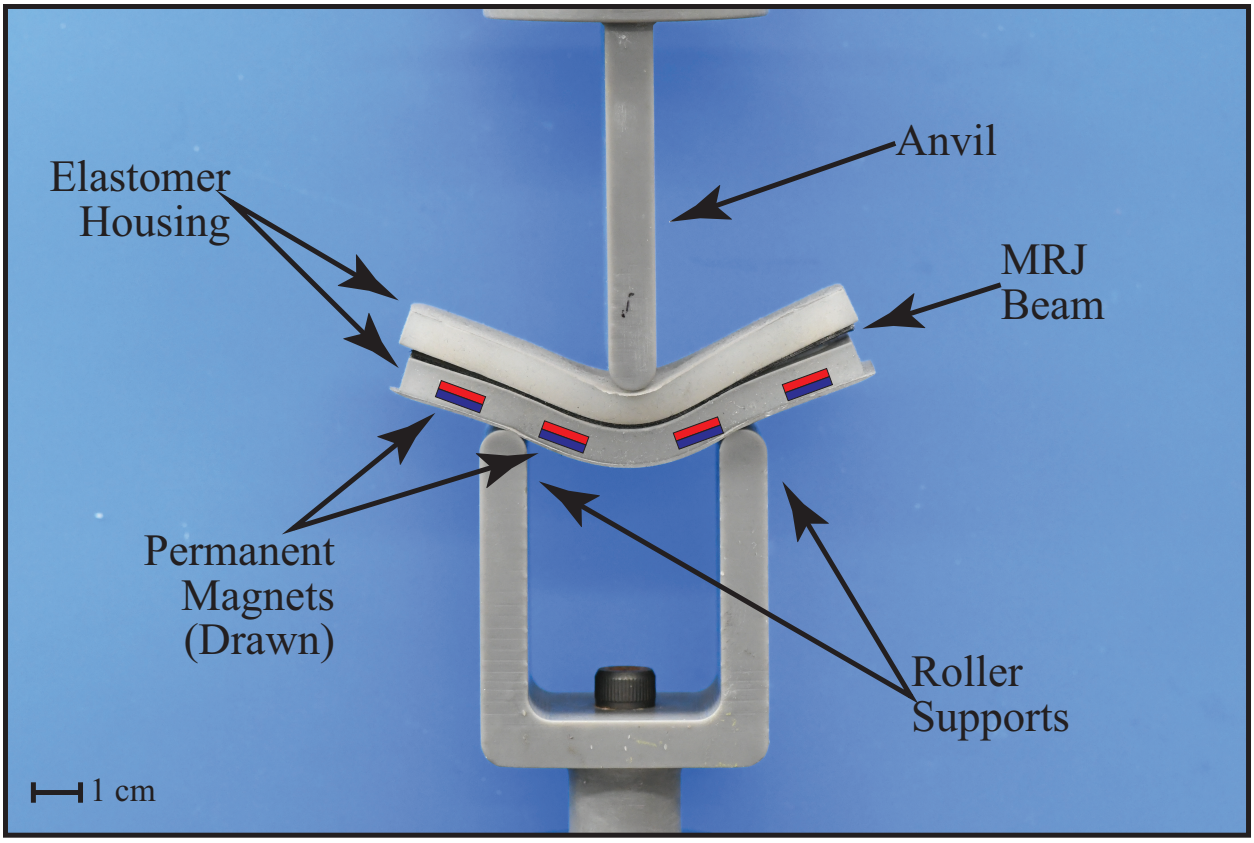

Figure S2: Testing apparatus with elastomer magnet housing used during experiments with an MRJ beam pictured at 7 mm of deflection. The anvil is pressing on the section of the sample not containing the permanent magnets.

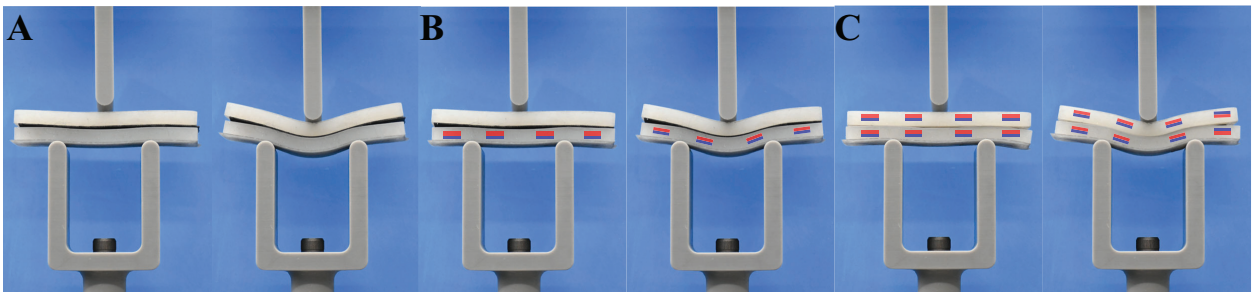

Figure S3: Pictures from testing MRJ beams without magnets (A), with a single row of magnets (B), and with a double row of magnets (C). For each case, the sample before and after testing is shown and the location of the magnets is represented by a drawing overlapped with the picture.

S2 Derivation of the Analytical Model

Our analytical model is adapted from pressure-based jamming models, originally formulated by Narang et al. [1], in which stacked layers (similar to what is used in the manuscript) are jammed together when vacuum pressure is applied. We further develop their model to take into account the effect of an applied external magnetic field by incorporating that a new fluid medium, magnetorheological fluid rather than air, is being used instead. This model applies to the layer-based scaffolding architecture, using the combined *MR and clutch effect* reported in the manuscript. One can see that the predicted stiffness of an MRJ beam varies depending on the MRJ beam base b (layer width), height h (layer thickness, layer number), and the frictional stress τ_f, which is found experimentally as a function of magnetic field (see Section 4.2 Magnetically Controlled Layers Cohesion Testing).

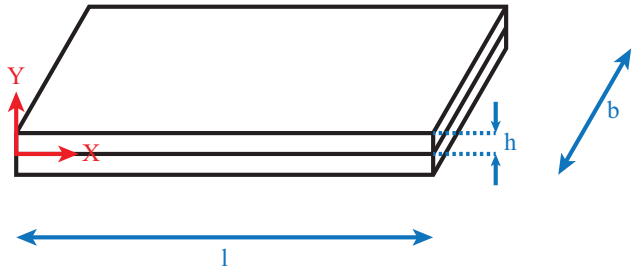

Figure S4: Two stacked layers with length l, width b, and height h, and the defined coordinate system overlayed.

We assume that the layers are slipping, such that the longitudinal shear stress along the stacked rectangular layers equates to the maximum frictional stress, τ_f. If we examine two layers, as illustrated in Fig. S4, with each having its own neutral axis, the axial strain fields can be represented by:

$$\epsilon_1(x,y) = -\kappa(x)y + A_1(x) \tag{S1a}$$
$$\epsilon_2(x,y) = -\kappa(x)y + A_2(x) \tag{S1b}$$

where κ is the curvature and $A_1(x)$ and $A_2(x)$ are the axial strain components. The stress fields can then be described by the following, in which E is the Young's Modulus:

$$\sigma_1(x,y) = -E\kappa(x)y + EA_1(x) \tag{S2a}$$
$$\sigma_2(x,y) = -E\kappa(x)y + EA_2(x) \tag{S2b}$$

Further, a single layer has the following moment-stress relationship, in which $\sigma(x,y)$ is the axial stress and S is the layer's cross-section.

$$M(x) = \int_S -\sigma(x,y)ydS \tag{S3}$$

Next, we substitute in the stress fields, Equations S2a and S2b, into Equation S3,

$$M(x) = 2\kappa(x)EI + (A_1(x) - A_2(x))EJ \tag{S4}$$

in which J is the first moment of the area and I is the second moment of the area of the layers' cross-section about the interface in between the layers.

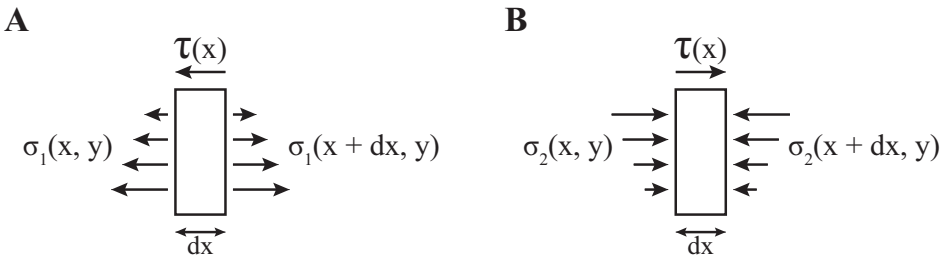

Figure S5: Static equilibrium of the bottom (A) and top (B) layers.

We then introduce the shear stress acting between layers, $\tau(x)$, from static equilibrium, as seen in Fig. S5. We then obtain the following force equations:

$$-\tau(x)bdx + \int_{S_1} \sigma_1(x+dx,y)dS_1 - \int_{S_1} \sigma_1(x,y)dS_1 = 0 \tag{S5a}$$

$$\tau(x)bdx + \int_{S_2} \sigma_2(x+dx,y)dS_2 - \int_{S_2} \sigma_2(x,y)dS_2 = 0 \tag{S5b}$$

Since we assume that the layers are slipping, $\tau(x)$ therefore equates to τ_f, and we can also substitute Equations S2a and S2b into Equations S5a and S5b, respectively.

$$-\tau_f b + EJ\frac{d\kappa}{dx} + Ebh\frac{dA_1}{dx} = 0 \tag{S6a}$$

$$\tau_f b - EJ\frac{d\kappa}{dx} + Ebh\frac{dA_2}{dx} = 0 \tag{S6b}$$

Since the sum of Equations S6a and S6b gives us the sum of the axial strain components equal to zero, or $A_1(x) + A_2(x) = 0$, we can substitute this into Equation S4 and obtain the governing equations, Equations S7 and S8.

$$M(x) = 2\kappa(x)EI + 2A_1(x)EJ \tag{S7}$$

$$-\tau_f b + EJ\frac{d\kappa}{dx} + Ebh\frac{dA_1}{dx} = 0 \tag{S8}$$

If we use the small deformation approximation, $\kappa(x) \approx \frac{d^2w}{dx^2}$ and integrate Equations S8 with respect to x, we then obtain the following:

$$M(x) = 2\frac{d^2w}{dx^2}EI + 2A_1(x)EJ \tag{S9}$$

$$A_1(x) = \frac{\tau_f x}{Eh} - \frac{J}{bh}\frac{d^2w}{dx^2} + C_1 \tag{S10}$$

in which C_1 is a constant from integration. From the Euler-Bernoulli beam theory, we know that

$$M(x) = \frac{Fx}{2} \tag{S11}$$

at $x = l/2$ during three-point bending [2, 3]. If we then equate Equations S9 and S11 with each other, we obtain the following:

$$\frac{Fx}{2} = 2\frac{d^2w}{dx^2}EI + 2A_1(x)EJ \tag{S12}$$

Next, we can substitute Equation S10 into Equation S12, and solve at deflection center, $x = l/2$, using the first moment of the area $J = \frac{bh^2}{2}$ and second moment of the area $I = \frac{bh^3}{3}$ for the layers' cross-section about the interface in between the layers.

$$\frac{Fx}{2} = 2\frac{d^2w}{dx^2}EI + 2\left(\frac{\tau_f x}{Eh} - \frac{J}{bh}\frac{d^2w}{dx^2} + C_1\right)EJ \tag{S13}$$

Given the following three-point bending boundary conditions at $x = 0$ and $x = l$

$$\frac{d^2w}{dx^2}(x = 0) = 0 \tag{S14a}$$

$$\frac{d^2w}{dx^2}(x = l) = 0 \tag{S14b}$$

we find $C_1 = 0$. We can then integrate Equation S13 and apply the slope boundary condition at $x = 0$, in which $\frac{dw}{dx} = \frac{-Fl^2}{16EI}$, to obtain the following:

$$\frac{dw}{dx} = \left(\frac{3F}{2Ebh^3} - \frac{3\tau_f}{Eh^2}\right)x^2 + C_2 \tag{S15}$$

Solving at $x = 0$ and applying the boundary condition, we find $C_2 = \frac{-Fl^2}{16EI}$. Integrating one final time and applying the deflection boundary conditions, $w(x = 0) = 0$ and $w(x = l) = 0$, we then achieve Equation S16.

$$w(x) = \left(\frac{F}{2Ebh^3} - \frac{\tau_f}{Eh^2}\right)x^3 - \frac{Fl^2}{16EI}x \tag{S16}$$

Substituting the second moment of inertia about its central axis for rectangular beam bending, $I = \frac{bh^3}{12}$, and the elastic modulus, $E = \frac{kl^3}{48I}$, we then achieve our final equation to model the MRJ beam stiffness.

$$k \propto \frac{F + bh\tau_f}{w}. \tag{S17}$$

Finally, to take into account the effects of the applied magnetic field, the maximum frictional stress is equal to μP, in which μ is the friction coefficient, and P is the applied pressure from the magnets. From the Magnetically Controlled Layers Cohesion Testing (Section 4.2 in the manuscript), we take the force obtained from the testing results, F, to be equal to the frictional force, or μN (N is the normal force). Dividing μN, or F, by the permanent magnet area, πr^2, then gives us the maximum frictional stress, τ_f.

S3 Electronically-Controlled Stiffening

The paper focuses on characterizing the change in stiffness of MRJ beams when exposed to a magnetic field. While we used permanent magnets for the characterizations presented in the paper for simplicity, magnetic fields can be generated electronically using electromagnets of electropermanent magnets. The proposed MRJ beams present significant stiffening tuning at relatively low magnetic fields (i.e., below 200 mT) with respect to other magnetically controlled stiffening strategies such as MREs [4, 5]. This feature can facilitate the integration of electronically controlled magnetic sources to tune the stiffness of the proposed MRJ beams.

Electronically-controlled stiffening was achieved by manufacturing four electro-permanent magnets (EPMs) that were embedded into an MRJ beam. The EPMs were evenly spaced 25.4 mm apart within the beam. The MRJ beam was made of thermoplastic elastomer and contained 1 ml of magnetorheological fluid with fibers scaffolding. The EPMs were individually controlled using an Arduino Mega to supply 5 A at 20 V to the exterior coils for 500 μs to switch from the OFF to ON states. The EPMs measure magnetic fields of 5 mT and 30 mT in the OFF and ON states, respectively.

A three-point bend test was employed on a tensile testing machine (5943, Instron) in both states, using the same testing setup reported in the manuscript (Fig. S2). No elastomer housing was used in this case because the EPMs were embedded into the MRJ beam. At a rate of 10 mm per minute, the anvil imposed a 5 mm displacement at beam center.

Results of these tests are illustrated in Fig. S6; the stiffness and forces required at maximum deflection are reported in Table S1. We observed a significant increase in the MRJ beam stiffness when the EPM is on.

It is interesting to notice that the 26% increase at 30 mT is consistent with the bending tests performed with permanent magnets and reported in Table 1 in the manuscript further highlighting how the stiffening tuning is independent of how the magnetic field is generated.

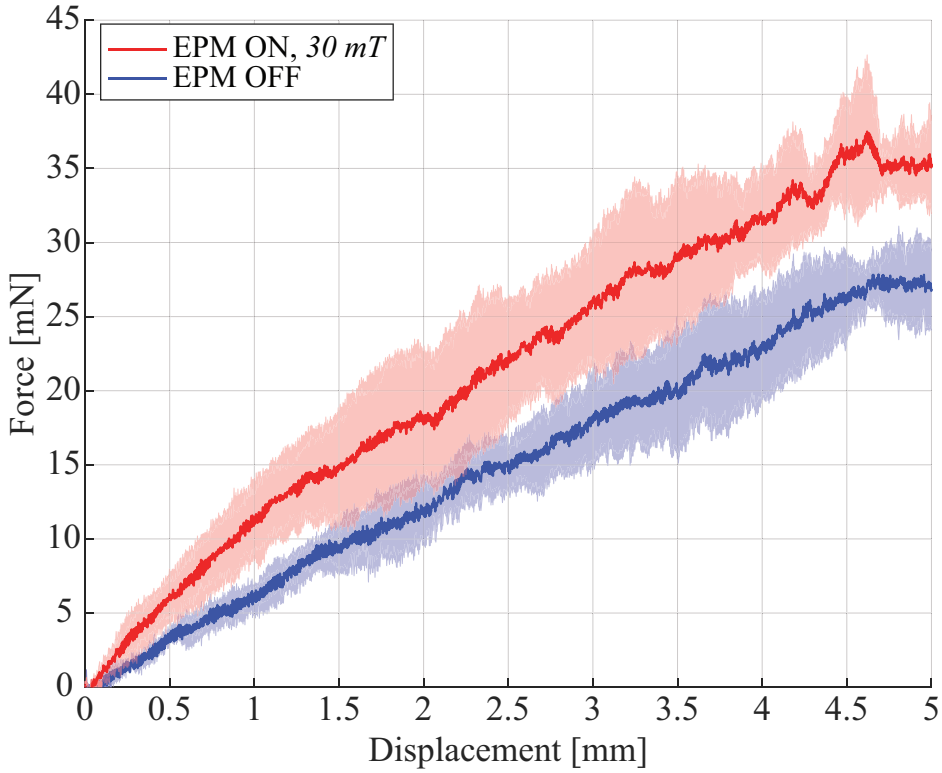

Figure S6: Force vs. deflection of an EPM-embedded MRJ beam with EPMs in ON and OFF states. Note that each curve is the mean of three trials and the shaded error bar represents one standard deviation.

EPM State	Magnetic Field (mT)	Stiffness (mN/mm)	Stiffness % Change	Force at Maximum Deflection (mN)	Force at Maximum Deflection % Change
OFF	5	6.38	—	31.05	—
ON	30	8.04	26.02%	43.45	39.94%

Table S1: Results of the three point bending test for the EPM-embedded MRJ beam in both OFF and ON states.

S3.1 Demonstration

An MRJ beam using fibers as the scaffolding architecture with four evenly-spaced EPMs embedded within was used to demonstrate electronically-controlled variable stiffening. This MRJ beam was centered upon two supports at its longitudinal ends. The center of the beam was given a prior deflection of 5 mm and then the four EPMs were toggled to their ON states, stiffening the beam into this configuration. A total mass of 70 g was placed at this initial deflection point, and the beam was able to hold the load. The EPMs were then turned to their OFF state, thereby decreasing the overall beam stiffness. As a result, the MRJ beam can no longer securely hold the 70 g mass and the load falls. This demonstration of electronically-controlled stiffening using an MRJ beam can be seen in Movie S1.

S4 Experiment with Water as the Fluid Medium

The *MR and clutch effect* presented in the paper provides significantly higher stiffening than the *MR effect* by itself. This is due to the added compression given by the double row of magnets diametrically positioned across the MRJ beams. To further understand the role of the magnetorheological fluid in the *MR and clutch effect*, experiments were run using the double row of permanent magnets and the four layer-based architecture samples using water as the fluid medium instead of the magnetorheological fluid. Using water as a medium allows us to isolate the component that is solely due to the pressure generated by the attraction between the magnets. The samples were fabricated in the same manner as described in the manuscript, but the 1 *ml* volume of magnetorheological fluid was replaced with an equal volume of water. The same three-point bend protocol described in the manuscript was employed and the results are plotted in Fig. S7. In Fig. S7 we can see how the increasing magnetic force causes indeed an increase in the stiffening of the samples. This increase in pressure generated by the magnets causes an effect that is analogous to the pressure-based stiffening generated with jamming architectures in soft robotics [6]. The test shows that this pressure-induced stiffening can also be induced via magnetic fields.

The comparison in stiffness between these samples and their respective MRJ counterparts is reported in Fig. S8 and numerical values are reported in Table S2. The use of magnetorheological fluids further enhances the stiffening significantly as shown in Fig. S8. Using magnetorheological fluid instead of water resulted in up to 43% increase in stiffening of the MRJ beams (see Table S2).

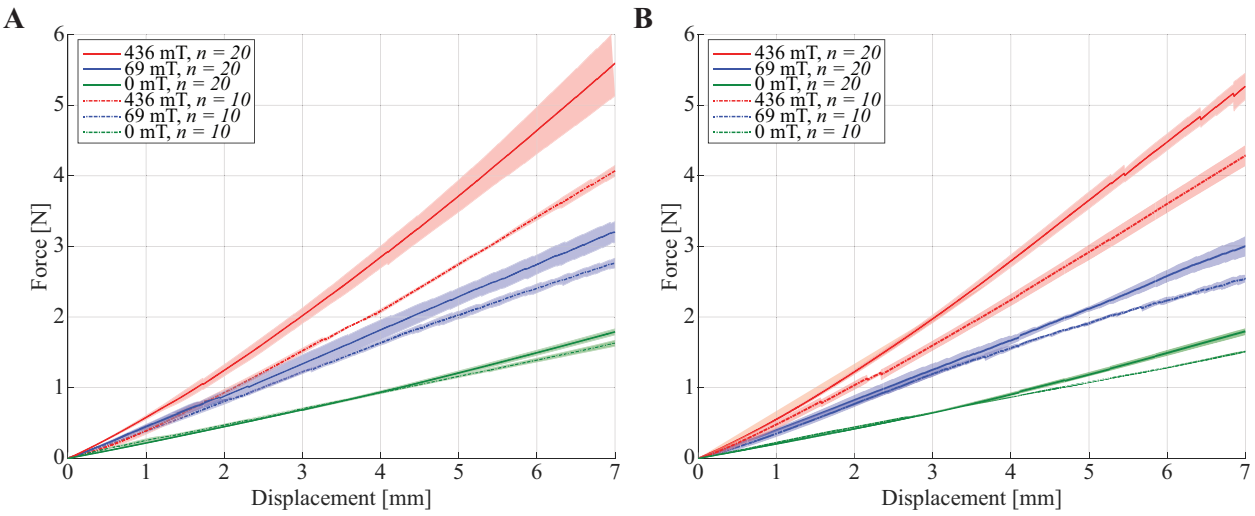

Figure S7: Force vs. deflection of beams with the layers-based scaffolding architecture and water as the fluid medium at three magnetic fields from the double row of magnets. The beam design patterns include (A) "Blank" design layers and (B) "Dots" design layers, with n = *layer number*. Each curve is the mean of three trials and the shaded error bar represents one standard deviation.

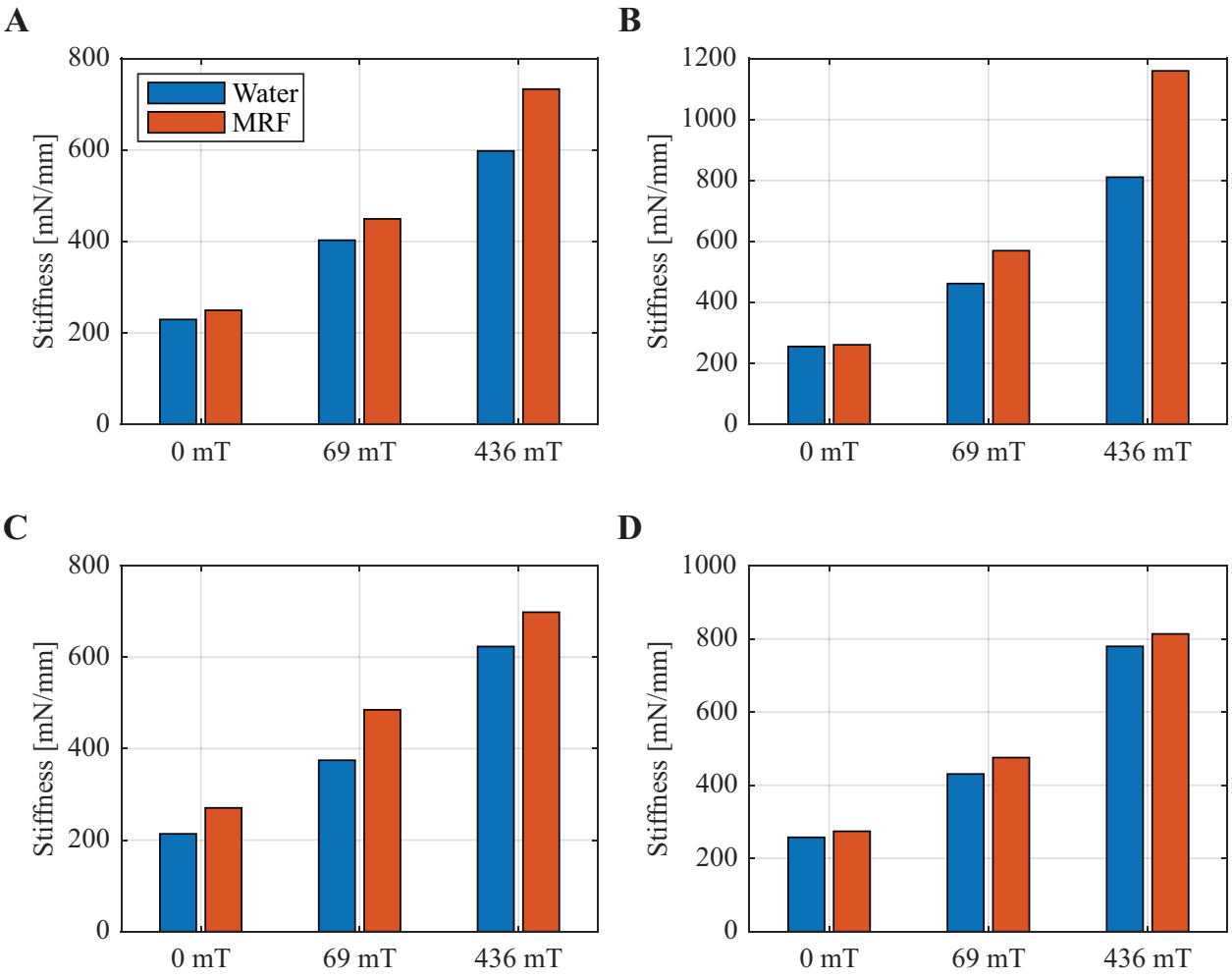

Figure S8: Stiffness comparison between samples using water as the fluid medium and their respective MRJ beam counterparts. The comparisons at three magnetic fields exhibiting the clutch effect are presented for: (A) "Blank" 10 layers, (B) "Blank" 20 layers, (C) "Dots" 10 layers, and (D) "Dots" 20 layers.

Scaffold Type	Magnetic Field (mT)	Water Stiffness (mN/mm)	MRJ Stiffness (mN/mm)	MRJ Stiffness % Increase
Blank - 10 Layers	0	229.39	249.47	8.75%
	69	402.78	449.51	11.58%
	436	597.99	733.28	22.62%
Blank - 20 Layers	0	255.42	261.05	2.20%
	69	461.94	569.85	23.36%
	436	810.99	1159.73	43.00%
Dots - 10 Layers	0	213.78	270.54	26.55%
	69	374.70	485.06	29.45%
	436	623.49	698.50	12.03%
Dots - 20 Layers	0	257.66	274.22	6.43%
	69	430.81	475.67	10.41%
	436	779.75	813.80	4.37%

Table S2: Results of the three point bending test for the double row of magnets case, i.e. clutch effect, using water as the fluid medium, with respective MRJ beam stiffness also tabulated for comparison. The percent increase in stiffness for the MRJ beams with respect to the ones with water is also reported.

References

[1] Y. S. Narang, J. J. Vlassak, and R. D. Howe, "Mechanically versatile soft machines through laminar jamming," *Advanced Functional Materials*, vol. 28, no. 17, pp. 1–9, 2018.

[2] R.C. Hibbeler, *Mechanics of Materials*, 10th ed. Hoboken, NJ: Pearson, 2017.

[3] O. A. Bauchau and J. I. Craig, *Euler-Bernoulli beam theory.* Dordrecht: Springer Netherlands, 2009, pp. 173–221. [Online]. Available: https://doi.org/10.1007/978-90-481-2516-6_5

[4] G. Y. Zhou, "Shear properties of a magnetorheological elastomer," Tech. Rep., 2003.

[5] M. R. Jolly, J. David Carlson, and B. C. MuñozMu, "A model of the behaviour of magnetorheological materials," Tech. Rep., 1996.

[6] B. Aktaş, Y. S. Narang, N. Vasios, K. Bertoldi, and R. D. Howe, "A modeling framework for jamming structures," *Advanced Functional Materials*, vol. 31, no. 16, pp. 1–15, 2021.